Molecular Immunology 136 (2021) 16–25

Contents lists available at ScienceDirect

Molecular Immunology

journal homepage: www.elsevier.com/locate/molimm

Extracellular crosslinking mass spectrometry reveals HLA class I – HLA class II interactions on the cell surface

Gad Armony [a,b], Albert J.R. Heck [a,b], Wei Wu [a,b,*]

[a] Biomolecular Mass Spectrometry and Proteomics, Bijvoet Center for Biomolecular Research and Utrecht Institute for Pharmaceutical Sciences, Utrecht University, Padualaan 8, 3584 CH, Utrecht, The Netherlands
[b] Netherlands Proteomics Centre, Padualaan 8, 3584 CH, Utrecht, The Netherlands

ARTICLE INFO

Keywords:
Extracellular crosslinking
Mass spectrometry
Human Leukocyte Antigen (HLA)
Plasma membrane interactions

ABSTRACT

Human Leukocyte Antigen (HLA) complexes are critical cell-surface protein assemblies that facilitate T-cell surveillance of almost all cell types in the body. While T-cell receptor binding to HLA class I and class II complexes is well-described with detailed structural information, the nature of *cis* HLA interactions within the plasma membrane of the surveyed cells remains to be better characterized, as protein-protein interactions in the membrane environment are technically challenging to profile. Here we performed extracellular chemical crosslinking on intact antigen presenting cells to specifically elucidate protein-protein interactions present in the external plasma membrane. We found that the crosslink dataset was dominated by inter- and intra-protein crosslinks involving HLA molecules, which enabled not only the construction of an HLA-centric plasma membrane protein interaction map, but also revealed multiple modes of HLA class I – HLA class II interactions with further structural modeling based on crosslinker distance restraints. Collectively, our data demonstrate that HLA molecules colocalize and can be densely packed on the plasma membrane.

1. Introduction

Proteins on the outer cell surface are critical determinants of cell-cell interactions and how cells respond to their surroundings. From mechanical support to signal transmission, many of these processes require multi-protein assemblies in the plasma membrane, for example integrins in focal adhesion (Sun et al., 2016), or T cell receptors and CD3 molecules in the immunological synapse (Alcover et al., 2018). In the specific case of GPCR activation, structural changes of plasma membrane proteins may also be required to kickstart a short pulse of downstream and intracellular signaling (Gurevich and Gurevich, 2017). Studying such membrane complexes with biochemical and structural methods is not easy since the extraction of membrane proteins from the native membrane environment could already alter their structure and interactions (Zhang and Cherezov, 2019). Therefore, which sample processing steps to use prior to structural measurements often requires a carefully deliberated choice, to maximize the preservation of the native protein complexes while minimizing possible artifacts.

To study membrane protein interactions under more native conditions, numerous indirect and visualization techniques have been applied. These include resonance energy transfer, protein-fragment complementation assays, and colocalization studies using super-resolution microscopy (Cui et al., 2019), all of which can make measurements while the protein complexes remain in the native membrane environment. Although these are very useful to report physical proximity between proteins, none of these methods can provide sufficient structural information needed to reveal interacting residues or structural models. Moreover, engineering of fluorescence reporters and two-hybrid tags for each plasma membrane protein to be studied is still a demanding bottleneck. Lastly, to be able to employ these methods, prior knowledge of the interaction or at least the identity of the interaction partners are still required.

In recent years, crosslinking mass spectrometry (XL-MS) has developed into a very promising method to study protein-protein interactions. Regardless of its application, to study purified protein complexes (Fernandez-Martinez et al., 2016; Leitner et al., 2012; Tüting et al., 2020) or

Abbreviations: HLA, Human Leukocyte Antigen; HLA-I, HLA Class I; HLA-II, HLA Class II; TCR, T-cell Receptor; XL-MS, Crosslinking Mass Spectrometry; DSSO, Disuccinimidyl Sulfoxide; SASD, Solvent Accessible Surface Distance; CSM, Crosslink Spectrum Match; SCX, Strong Cation Exchange.

* Corresponding author at: Biomolecular Mass Spectrometry and Proteomics, Bijvoet Center for Biomolecular Research and Utrecht Institute for Pharmaceutical Sciences, Utrecht University, Padualaan 8, 3584 CH, Utrecht, The Netherlands.
E-mail addresses: g.armony@uu.nl (G. Armony), a.j.r.heck@uu.nl (A.J.R. Heck), w.wu1@uu.nl (W. Wu).

https://doi.org/10.1016/j.molimm.2021.05.010
Received 1 February 2021; Received in revised form 23 April 2021; Accepted 19 May 2021
Available online 27 May 2021

proteome-wide interactome studies (Bartolec et al., 2020; Chavez et al., 2018; Liu et al., 2018b), XL-MS relies on small bifunctional reagents (crosslinkers) to covalently connect between residues (usually lysine) in close proximity. By reliable crosslinker fragmentation during mass spectrometry analysis (Klykov et al., 2020; Liu et al., 2018a, 2017), both the identity of the crosslinked proteins as well as the positions of the crosslinked residues can be simultaneously uncovered in one mass spectrometry experiment. In addition, the crosslinked positions reveal valuable structural information that may be used to model the architecture of protein complexes, since the distance between crosslinked residues must be shorter than the length of the crosslinker used. In other words, the crosslinker length places a distance restraint that can be used to model structures of a protein, or a protein complex. When the crosslinked positions are on the same protein, an intra-link, the distance restraint may provide information about the tertiary structure of the protein. When the crosslinked positions are on different proteins, an inter-link, it provides information about the quaternary structure of a protein complex which can be used to assist in elucidating the binding interface through molecular docking (van Zundert et al., 2016; Vreven et al., 2018; Webb and Sali, 2016; Yang et al., 2015). Collectively, the combination of interacting protein identities, site-specific evidence, and distance restraints make XL-MS a valuable method to directly assemble the structure of protein complexes.

In this work, we applied extracellular XL-MS to an antigen presenting JY cell line, to probe the plasma membrane interactions that enable its immunological function. On the JY cell surface, both main classes of Human Leukocyte Antigen (HLA) proteins present short peptide fragments to CD4+/CD8+ T-cells for immune surveillance, by binding to T cell receptors (TCRs) and CD4/8 co-receptors. The HLA class I (HLA-I) complexes consist predominantly of the allotypes HLA-A, HLA-B, and HLA-C that are membrane-anchored, and each complexed with a free β2M subunit, whereas the HLA class II (HLA-II) complexes consists of dimeric assemblies of HLA-IIα and HLA-IIβ that are both membrane-anchored. While the bases for HLA-TCR, HLA-CD8, and HLA-CD4 *trans* interactions are well characterized with detailed structural information (Cole et al., 2017; Gao et al., 1997; Yin et al., 2012), *cis* HLA interactions within the plasma membrane of the surveyed cells, which can modulate the dynamics of T-cell recognition, are not as well-documented. The data we present here thus provide critical structural information to model different modes of HLA interactions.

2. Material and methods

2.1. Whole-cell extracellular crosslinking

JY cells were cultured in RPMI 1640 media (Lonza, Switzerland) supplemented with 10 % fetal bovine serum (GE Healthcare, IL, USA), 10 mM L-glutamine, 50 U/mL penicillin and 50 ug/mL streptomycin, at 37 °C in a humidified incubator supplemented with 5 % CO_2. In two separate experiments, 2.5×10^8 cells were harvested each by centrifugation at 1000 *g* for 1 min then gently washed four times with 50 mL warm PBS. Cells were further washed with 20 mL crosslinking buffer (50 mM HEPES pH 7.8, 150 mM NaCl), and resuspended in crosslinking buffer at a density of 10^8 cells/mL. The cell density was carefully titrated to ensure minimal artifacts due to high cell density. The chemical crosslinker reagent Disuccinimidyl sulfoxide (DSSO) was added to a final concentration of 1 mM, and cell suspension was crosslinked for 15 min with gentle end-to-end inversion at room temperature. The crosslinking reaction was quenched with 10 mM Tris pH 8.5 for 10 min. Crosslinked cells were then pelleted at 2000 *g* for 1 min (with slow deceleration) and snap-frozen in liquid nitrogen.

2.2. Plasma membrane fractionation

Plasma membrane was enriched using a membrane fractionation kit (ab65400, Abcam, Cambridge, UK) as described previously (Mezzadra et al., 2017). All steps were performed at 4 °C or on ice. Briefly, the crosslinked cell pellets were thawed, and gently resuspended in isotonic and detergent-free homogenisation buffer supplemented with 1 × cOmplete protease inhibitors (Roche Diagnostics, Switzerland), 50 μg/mL DNase I (Sigma-Aldrich, MO, USA), and 50 μg/mL RNase A (Sigma-Aldrich). Cells were disrupted manually with a hand-held glass homogeniser. Cells that remained intact were pelleted at 700 *g*, for 10 min, and discarded. From the supernatant, total membranes were pelleted at 10,000 *g*, for 30 min, and further partitioned in partially miscible gradients established by mixing 200 μl each of the upper and lower phase solutions (Abcam ab65400). Plasma membrane proteins were retrieved from the upper phase and precipitated, for 30 min, by 5 times dilution with ultra-pure water. Plasma membrane proteins were then pelleted at 20,000 *g*, for 30 min, resuspended in 8 M Urea, 50 mM Ammonium bicarbonate, 0.2 % Sodium deoxycholate, and then snap-frozen in liquid nitrogen.

2.3. Proteolytic digestion

The protein content of plasma membrane lysates was estimated with a Bradford assay (BioRad, CA, USA). 240 μg of plasma membrane proteins were reduced with 4 mM Dithiothreitol (DTT) for 60 min, alkylated with 16 mM Iodoacetamide (IAA) for 30 min in the dark which was then quenched with another 4 mM DTT. Alkylated proteins were diluted 5 times with 50 mM Ammonium bicarbonate, and digested with Lys C (ratio 1:75; Wako, Japan) and Trypsin (ratio 1:50; Sigma-Aldrich, MO, USA) at 37 °C for 16 h. Digested peptides were acidified to 5 % Formic acid and centrifuged at 20,000 *g* for 10 min. The clear supernatant was desalted using Sep-Pak C18 cartridge (Waters, MA, USA), vacuum-dried, and stored at −80 °C.

2.4. Strong cation exchange (SCX) chromatography

The desalted peptides were dissolved in 10 % formic acid, 2 % DMSO and loaded on a Luna 100A SCX column (50 mm × 2 mm, 5 μm, Phenomenex product number 00B-4398-B0) with the help of a C18 Opti-Lynx trap column (4.6 mm × 5 mm, 49 μm, Optimize Technologies product number 11-02874-TA). Solvent A consisted of 0.05 % formic acid, 20 % acetonitrile in water and solvent B consisted of 0.05 % formic acid, 20 % acetonitrile, and 0.5 M NaCl. The SCX gradient was: 0–10 % B in 10 min, 10–40 % B in 15 min, 40–80 % B in 5 min, 80–100 % B in 20 min, 100 % B for 10 min. One-minute fractions were collected and pooled into 20 approximately equal fractions by mean UV intensity. The pooled fractions were desalted with Oasis HLA 96-well μElution plate (Waters, MA, USA), vacuum-dried and stored at −80 °C.

2.5. Liquid chromatography with tandem mass spectrometry (LC–MS/MS)

Desalted SCX fractions were analyzed in triplicates by reversed-phase (RP) LC–MS/MS with an UHPLC 1290 system (Agilent, CA, USA) coupled to an Orbitrap Fusion mass spectrometer (Thermo Fischer Scientific, CA, USA). Peptides were trapped on a homemade 2 cm ×100 μm pre-column packed with Reprosil C18 (3 μm) and separated on a homemade 50 cm ×75 μm column packed with Poroshell EC-C18 (2.7 μm). The resolving gradient was established by mixing solvent A (0.1 % formic acid) and solvent B (0.1 % formic acid, 80 % acetonitrile). To maximize peptide separation in each fraction, the resolving gradients varied between 5–32 % Solvent B to 8–39 % Solvent B. The gradient was as follows: 5 min at 100 % A (trapping), 97 min resolving gradient, 2 min up to 100 % B, 5 min hold at 100 % B, 1 min lower to 100 % A, 10 min equilibrate for next sample at 100 % A. In all cases, the flow was passively split to ~200 nL/min.

MS1 was performed at 60,000 resolution, from 310 to 1600 m/z, after accumulation of 5×10^5 ions (125 %) in a maximum injection time of 50 ms. Top 10 most intense precursors with a minimum intensity of

2×10^4 and a charge of 3–8 were selected for MS2 by CID fragmentation (30 % collision energy). MS2 was performed using the orbitrap at 30,000 resolution with automatically defined *m/z* range (normal setting) and 5×10^4 AGC target (100 %), in a maximum injection time of 54 ms. Signature peaks of DSSO (a targeted mass difference of 31.9721) were selected for MS3 and fragmented by HCD (30 % collision energy). MS3 was performed using the ion trap in rapid mode, automatically defined *m/z* range (normal setting) and 10^4 AGC target (100 %) in a maximum injection time of 150 ms.

2.6. Database search

The raw MS data was processed with Proteome Discoverer 2.4 (version 2.4.1.15) using the integrated XlinkX nodes. The DSSO_MS2_MS3 analysis template was used with the following modifications: minimum precursor mass 350 Da and minimal peptide mass of 300 Da; two peptides were considered for each spectrum; deamidation on N/Q and N-terminal acetyl were added as variable modification. Data of each of the six replicates (two biological experiments measured in triplicates) was grouped in a processing workflow which were all under the same consensus workflow. The data was searched against the SwissProt human database (downloaded on 09/2019, containing 20,442 protein sequences, curated to match the JY HLA type – A*02:01, B*07:01, C*07:01, DRA*01:01, DRA*01:02, DRB1*04:01, DRB1*13:01, DQA1*01:03, DQA1*03:01, DQB1*03:02, DQB1*06:03, DPA1*01:03, DPB1*02:01, DPB1*04:01 (see first 17 sequences in the database file deposited to PRIDE, identifier PXD022675). Signal peptides and mitochondrial transit peptides as annotated in UniProt were removed to allow for correct mapping of crosslinks to the mature N-terminus, but residue numbers for all proteins remained as annotated in the UniProt sequence database.

2.7. Visualization

Crosslinking maps were constructed with proteins detected by at least 2 CSMs, using CrossID (de Graaf et al., 2019) or xiNET(Combe et al., 2015). Solvent accessible surface distances were calculated using Jwalk (Bullock et al., 2016). Molecular models were aligned and visualized using either Pymol 2.5 or UCSF chimera 1.14rc.

2.8. Molecular docking

The structures of HLA-I A2 (PDB ID 1HHI) and HLA-II DR (PDB ID 5NI9) were used to represent HLA-I and HLA-II, respectively. DisVis webserver (van Zundert et al., 2017; van Zundert and Bonvin, 2015) was used to check compatibility between crosslinks for HLA-I to HLA-II. Molecular docking was performed with HADDOCK 2.4 web-service (van Zundert et al., 2016). The docking was guided by ambiguous restraints based on DisVis interaction prediction (over 0.5) and unambiguous restraints based on the crosslinks, supplemented with a restraint between two atoms placed at the membrane facing side of the HLA structures to represent being tethered to the same membrane. The default parameters of HADDOCK were used except for the energies of ambiguous restraints which were reduced to 0.3 of their default values. The HADDOCK structures were scored based on the crosslinks solvent accessible surface distances (SASDs) using XLM tools (Sinnott et al., 2020). The best docking models were picked based on both the HADDOCK clustering and the cMNXL score (Bullock et al., 2016).

2.9. Sequence alignment

HLA sequences were aligned using Clustal Omega webservice (Madeira et al., 2019).

2.10. Immunoprecipitation and western blot

For reciprocal IP, 3.6×10^8 JY cells were lysed with 15 ml Pierce IP lysis buffer (Thermo Fischer Scientific, MA, USA) supplemented with 1 × cOmplete protease inhibitors (Roche Diagnostics, Switzerland), 50 μg/mL DNase I (Sigma-Aldrich, MO, USA), and 50 μg/mL RNase A (Sigma-Aldrich) for 30 min at 4 °C. The lysate was cleared by centrifugation at 20,000 *g* for 10 min at 4 °C and protein concentration was determined with Pierce BCA assay (Thermo Fischer Scientific). HLA-I or HLA-II were immunoprecipitated at 4 °C for 21 h, from 25 mg of lysate, with 125 μL of Protein A/G beads (Santa Cruz, TX, USA) coated with 0.5 mg antibody, W6/32 (gift from Prof. Dr. Stefan Stevanović) or B8-11-2 (Bioceros, The Netherlands) respectively. The beads were washed with Pierce IP lysis buffer, eluted with 750 μL IgG elution buffer (Thermo Fischer Scientific) and neutralized with 45ul of 1 M Tris pH 9.5. The elution fractions were subsequently depleted from contaminating antibodies using 125 μL protein A/G beads at 4 °C for 20 h, then concentrated to 60 μL using a 10,000 MWCO filter (Millipore, MA, USA).

HLA-I and HLA-II co-immunoprecipitated proteins, together with 1 μg JY cell lysate, were separated by SDS-PAGE, and transferred to PVDF membrane. Blocking was performed with 5 % non-fat milk in TBST at room temperature. W6/32 primary antibody was used at 1.25 μg/mL, while HRP-conjugated goat anti-mouse secondary antibody (Dako, Denmark) was used at 1:2,500 dilution. HRP signal was visualized with Pierce ECL reagent (Thermo Fischer Scientific).

3. Results

3.1. Whole-cell extracellular crosslinking

To obtain an unbiased plasma membrane interactome, our strategy was to perform chemical crosslinking on intact cells, and rely on two sequential fractionation procedures to boost the eventual detection of crosslinked peptide pairs by mass spectrometry (Fig. 1). With the clear focus on extracellular interactions, we chose to perform the chemical crosslinking with disuccinimidyl sulfoxide (DSSO) which does not readily cross cell membranes (Staros, 1982). This should largely prevent abundant intracellular proteins from consuming the crosslinkers (Fürsch et al., 2020), and increase the effective crosslinker concentration in the extracellular space, where our main interest lies (Fig. 1A). DSSO is also MS cleavable, thereby facilitating confident identification of crosslinks by combining mass spectrometry evidence at both MS2 and MS3 levels. With a double fractionation, first for plasma membrane proteins, and then for crosslinked peptide pairs from digested plasma membrane proteins (Fig. 1B), we aim to reduce the sample complexity prior to LC–MS analysis, to further boost selectivity and sensitivity of detecting crosslinks. We chose strong cation exchange (SCX) chromatography for pre-fractionation of crosslinked peptides (Fig. 1B), since SCX has been a reliable method to separate crosslinked peptides with higher charge and has been widely-adopted for deeper proteome-wide crosslinking analyses (Albanese et al., 2020; Chen et al., 2010; Fritzsche et al., 2012; Rinner et al., 2008).

Employing such a strategy (Fig. 1), we crosslinked the external surface of JY cells to map the extracellular interactions between plasma membrane proteins. This led to the identification of 334 unique inter-link crosslinks between 317 different proteins, and 543 intra-link crosslinks between proximal residues on the same protein. As expected, compared to proteins identified from a whole-cell lysate, we significantly enhanced the detection of proteins annotated with membrane-associated keywords (Fig. 2A). This provided confidence that our workflow has good specificity, and can boost the MS intensity and likelihood of detecting crosslinks of extracellular proteins. From the large number of intra-links identified, we further checked the proximity of crosslinked residues (in red) on the surface of four well-documented plasma membrane proteins (Fig. 2B). In particular for the LAT1 transporter, crosslinks were detected only on the extracellular domain; no

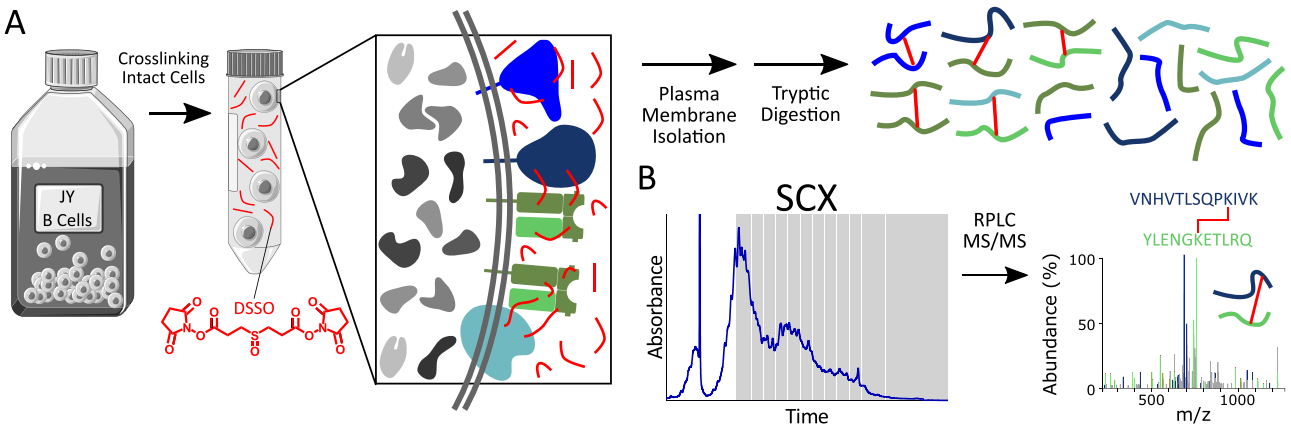

Fig. 1. Extracellular crosslinking. (A) Crosslinking mass spectrometry (XL-MS) strategy. JY cells grown in suspension were harvested, and whole cells were resuspended in PBS containing DSSO for extracellular crosslinking. Plasma membrane material was isolated from crosslinked cells, and digested for subsequent purification of crosslinked peptide pairs by strong cation exchange (SCX) chromatography. **(B)** SCX pre-fractionation and LC–MS/MS analysis. Crosslinked peptides were collected from SCX fractions. Peptides in each fraction were further analyzed by reversed-phase LC–MS/MS and identified using Proteome Discoverer with the XlinkX node.

crosslinks were detected in the intracellular domain, although non-crosslinked peptides from the intracellular region were detectable before SCX enrichment. Together, these provide further confidence that plasma membrane integrity was not breached during the extracellular crosslinking procedure, and that the DSSO did not cross the plasma membrane (Supplementary Fig. A.1). By calculating solvent accessible surface distance (SASD) on these four presented structures (Fig. 2B), we validated that the crosslinked residues are largely within 34 Å, the maximal distance DSSO can span (Fig. 2C, top). All the crosslinked residues were also within expected distances apart by considering direct Cα-Cα Euclidean distances, as an alternative measure (Fig. 2C, bottom). Collectively, these data demonstrate the feasibility of whole-cell extracellular crosslinking as a strategy to study interactions on the external cell surface.

3.2. Cell surface HLA interactome

Amongst all the plasma membrane proteins identified with crosslinks, HLA proteins contributed significantly with a total of 100 crosslinks containing either HLA-I or HLA-II as one of the crosslinked proteins. This is concordant with the documented high abundance of HLA proteins on the JY cell plasma membrane (Neumann et al., 2013), and makes HLA proteins a relevant starting point to nucleate plasma membrane interaction networks on these cells (Fig. 3A). Notably, within these 100 crosslinks, more than half were identified either between HLA-I molecules, between HLA-II molecules, or between HLA-I and HLA-II molecules (Supplementary Tables A.1–A.3), leading us to conclude that the most prominent HLA interactor on the plasma membrane is another HLA molecule. Crosslinks usually originate from the abundant complexes (Fürsch et al., 2020) and any crosslink formed by a random proximity is not likely to generate enough copies of the crosslinked peptides to be identified. Therefore, the data suggests that higher-order HLA complexes are likely to be present frequently and abundantly on the plasma membrane surface of JY cells.

Next to interactions between HLA proteins, a number of other plasma membrane proteins (e.g. CD48, CD59, CD53, ICAM1, TFRC, and SLC3A2) were also detected as crosslinked to HLA proteins (Fig. 3A, outer ring). Some of these interactions have been hinted at previously by other methods, for instance, using affinity-purification mass spectrometry methods (Huttlin et al., 2020, 2017) or cytometry and imaging methods (Bene et al., 1994; Lebedeva et al., 2004; Szöllósi et al., 1996). Nevertheless, in these reported studies the proposed interactions were not characterized structurally and no interaction domain or site information was established. The simultaneous detection of many such reported plasma membrane interactions in our whole-cell crosslinking approach indicates that our strategy is reliable and coherent with findings in existing studies, with the added value of directly obtaining structural information about these complexes.

By mapping the crosslinked positions on these plasma membrane HLA-interactors, the directionality and topology of interactions may be rationalized. For instance, two crosslinks between the transferrin receptor TFRC (K585; K177) to HLA-I (both to K92) seem to support the same mode of interaction, since both residues on TFRC are on the same interaction face (Supplementary Fig. A.2). When crosslinked positions are far apart on the protein structure, for instance on the extracellular domain of LAT1 (K615 and K266), it is then more likely that an HLA molecule approach LAT1 from either one of two sides (Supplementary Fig. A.2). Such guided interpretations of the interaction may benefit the structural analysis of multimeric assemblies and protein complexes between partners with high sequence homology.

3.3. HLA class I – HLA class I interactions

Multimeric states of HLA proteins have been inferred previously in several studies (Lavi et al., 2012; Matko et al., 1994; Szöllósi et al., 1996), some dating over 20 years ago. Yet, there is still neither consensus nor resolution achieved regarding the contact sites and modes of interaction. Part of the difficulty in determining these rises from the high sequence and structural similarity between the HLA proteins (Supplementary Figs. A.3, A.4) in the same complex. For instance, the sequence similarity between HLA-A, HLA-B, and HLA-C is as high as 89 %, with 75 % sequence identity, where about 12 % of the sequence codes for the variable peptide binding groove. In terms of three-dimensional structure, HLA-A, HLA-B, and HLA-C are also almost identical with RMSDs of less than 3 Å between these structures. Such an extent of similarity makes it very difficult to distinguish HLA-A homodimers from heterodimers of HLA-A, HLA-B, and/or HLA-C.

In this study, we relied on the unique sequences in the crosslinked peptide pairs to assign unique crosslinks between different HLA-I proteins. This is possible with single amino acid resolution. For instance, HLA-A was detected to be crosslinked to HLA-B (sequence [K]WEAAR) and HLA-C (sequence [K]LEAAR) (Supplementary Table A.1). Furthermore, we could also identify interactions shared by all HLA-I allotypes expressed in JY cells (A*02:01, B*07:02, C*07:02). For instance, β2M was crosslinked to K145 of HLA-A, HLA-B, and HLA-C separately (sequences GYHQYAYDG[K]DYIALK, LLRGHDQYAYDG[K]DYIALNEDLR, and GYDQSAYDG[K]DYIALNEDLR respectively), as evidenced by three different peptides connected by DSSO to position 21 of β2M

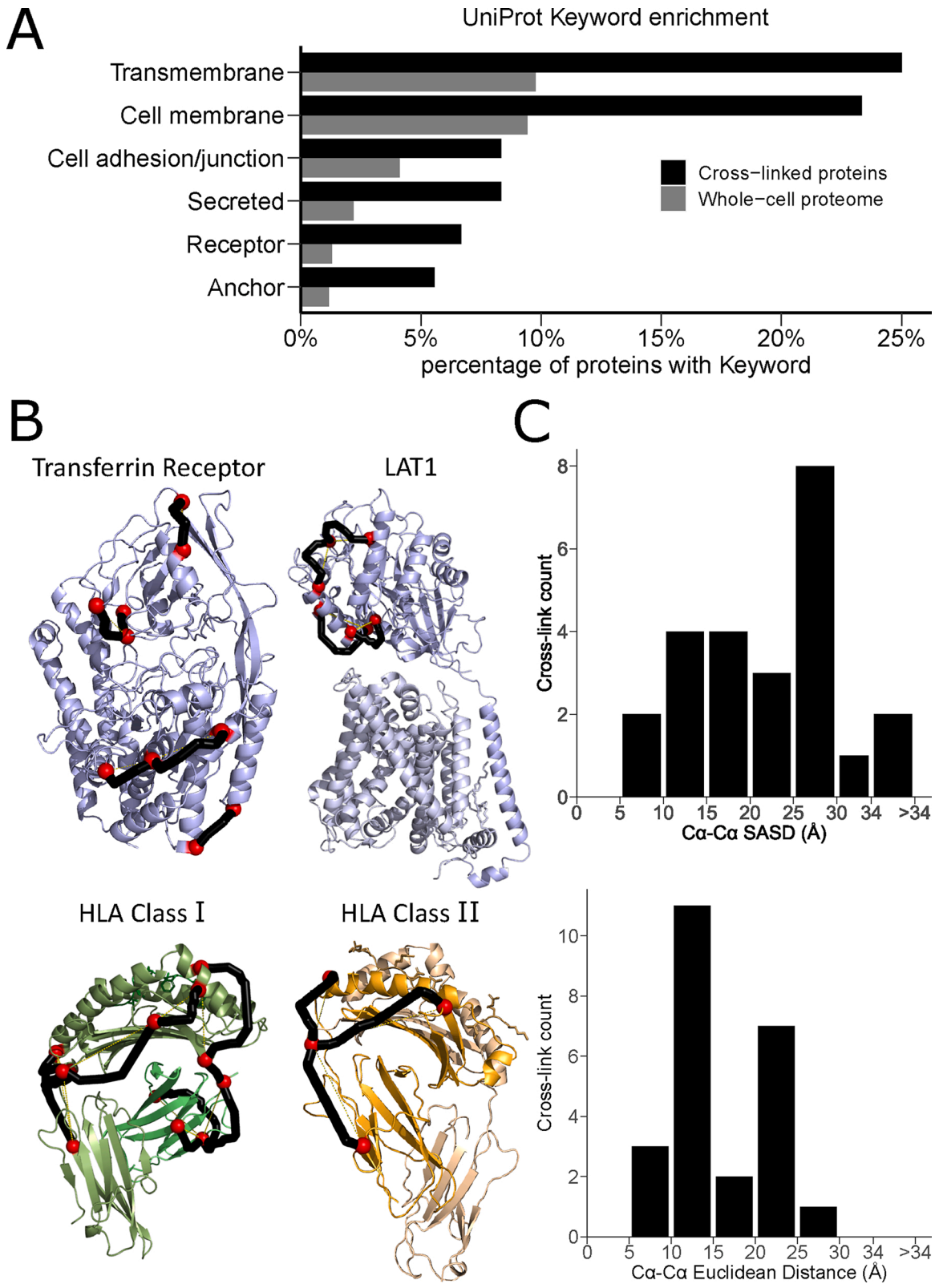

Fig. 2. Validation of plasma membrane crosslinks. (A) Validation of plasma membrane enrichment using UniProt Keywords for the proteins identified by crosslinks, when compared to protein identifications in the whole-cell proteome. **(B)** Mapping of intra-links on plasma membrane proteins with reported structures. Solvent accessible surface distances (SASDs) between intra-link positions were visualized as black tubes between crosslinked residues (red spheres) on reported PDB structures. SASD was calculated with Jwalk, and visualized on the structures of Transferrin receptor (PDB ID: 1CX8), LAT1 amino acid transporter (PDB ID: 6IRS), HLA Class I (PDB ID: 1HHI), and HLA Class II (PDB ID: 5NI9). **(C)** Binned distances of crosslinks mapped in (B). *Top*, SASDs; *Bottom*, Cα-Cα Euclidean distances.

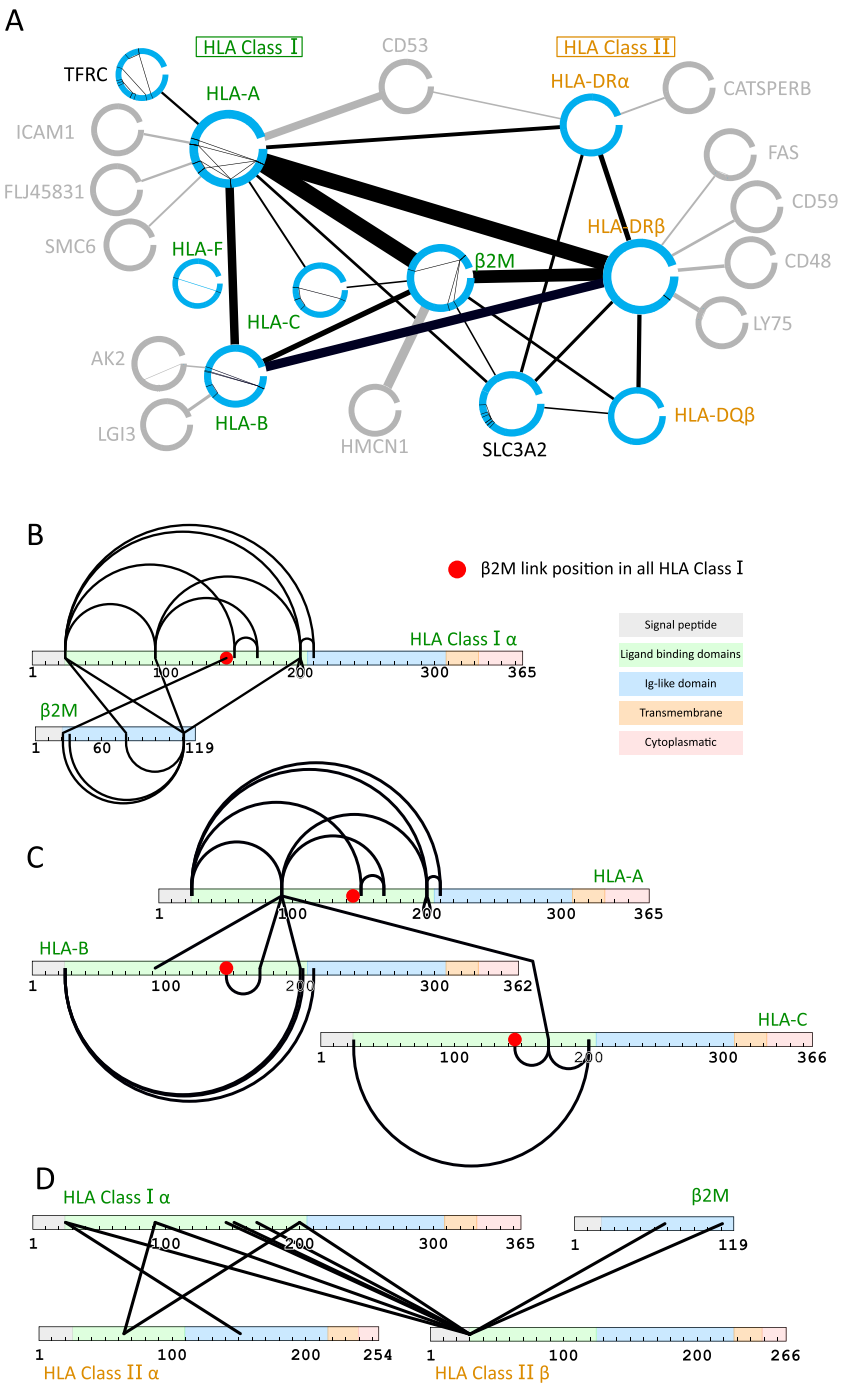

Fig. 3. HLA interactome map as defined by XL-MS. (A) Overview of proteins crosslinked to HLA proteins. Proteins detected with crosslinks to HLA proteins (≥2 Crosslink Spectra Matches, CSMs) are visualized by CrossID, in a map centered around the HLA class I (green) and HLA class II (blue) molecules. The size of the nodes represents number of interlinks. Lines within each node indicate intra-links. Line thickness between nodes represents the number of CSMs. **(B)** Crosslinks between HLA-A and β2M subunits. Structural and functional domains are annotated by color. Unique crosslinks are visualized as black lines. Red circle marks a position on all HLA-I types with equivalent crosslinks to β2M. **(C)** Crosslinks observed between HLA-A, HLA-B and HLA-C. Red circle marks a position on all HLA-I types with equivalent crosslinks to β2M. **(D)** Crosslinks between HLA class I and HLA class II, regardless of the HLA-I or HLA-II type. See Tables A.1–A.3 for further details.

(Supplementary Table A.1). Such interactions would thus be equivalent since β2M is crosslinked to equivalent positions on all HLA-I allotypes.

By systematically dissecting sequence information of crosslinked peptide pairs, we generated a comprehensive list of crosslinking sites and equivalent interactions between HLA-I proteins (Supplementary Table A.1), and illustrated these in Fig. 3B, C. We further arrived at a non-redundant set of crosslinked residues between HLA-I molecules by retaining crosslinks that can only be inter-protein. These would be links that either connect two distinct HLA allotypes or connect residues that are more than 45 Å apart on the same allotype (these cannot be intra-links, since SASD within the same molecule exceeds length of DSSO) (Supplementary Table A.2). This adds residue-level resolved information to existing reports of HLA-I – HLA-I interactions (Dirscherl et al., 2018; Matko et al., 1994; Szöllősi et al., 1996) and provides structural coordinates as orthogonal evidence of such interactions.

3.4. HLA class I – HLA class II interactions

Unlike the HLA-I proteins that form the complex by association with the free β2M subunit, HLA-II complexes are formed by the dimerization of HLA-IIα and HLA-IIβ. In our data, both HLA-IIα and HLA-IIβ were detected as crosslinked to HLA-I and β2M at multiple positions, providing ample evidence that HLA-I – HLA-II complexes are prevalent on the plasma membrane (Fig. 3D, Supplementary Table A.3). In addition, we also verified that HLA-I proteins co-immunoprecipitate abundantly with HLA-II by reciprocal immunoprecipitations with an anti-HLA-DR antibody (Fig. 4A). Using the same strategy described to consolidate equivalent HLA-I – HLA-I crosslinks, we also obtained a set

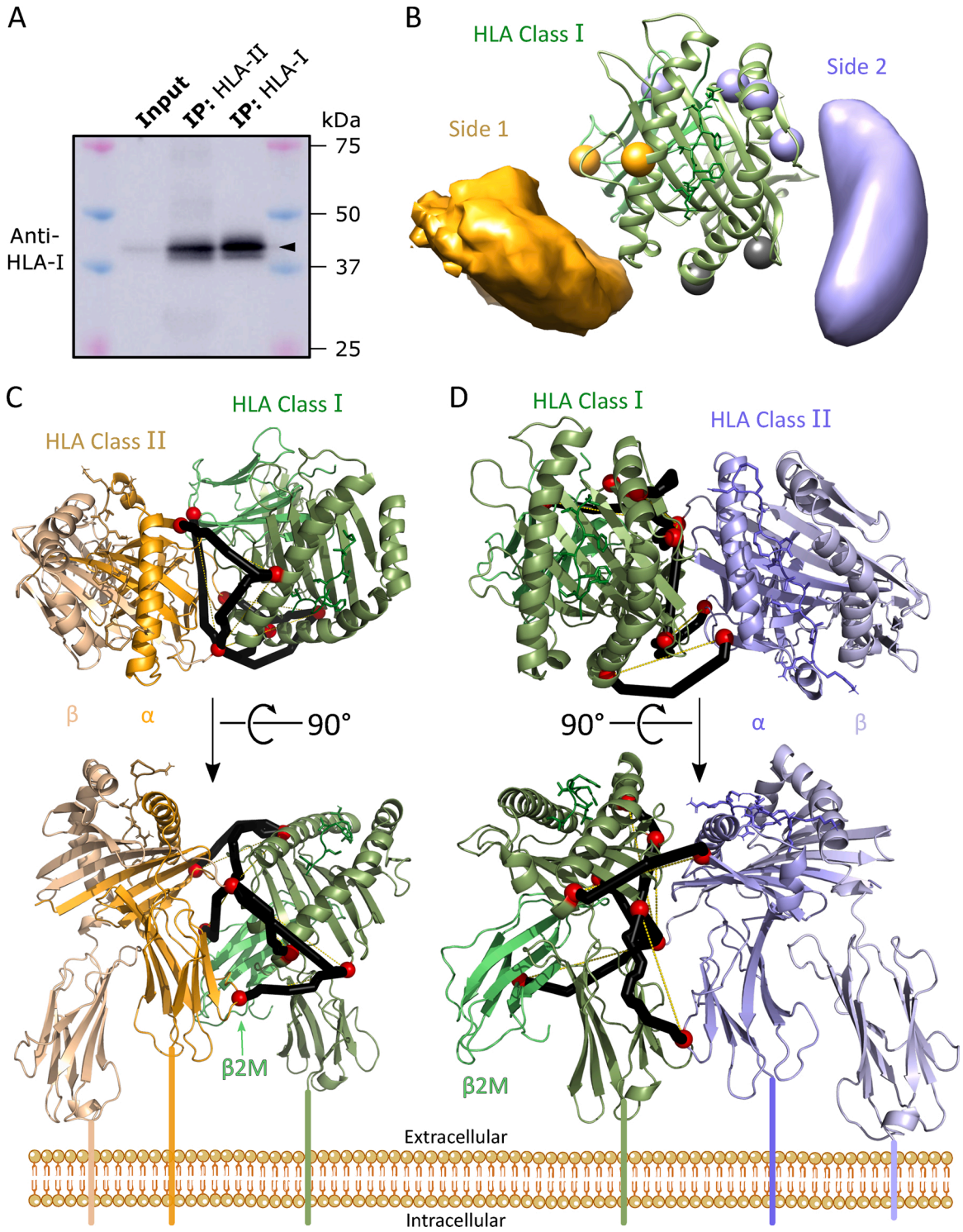

Fig. 4. HLA class I and HLA class II docking models. (A) Reciprocal IP with HLA-II antibody. HLA-I co-immunoprecipitated with HLA-II was detectable by western blot using a pan-HLA-I antibody. **(B)** Two possible modes of HLA-II interactions with HLA-I. On HLA-I green ribbon structure (PDB ID: 1HHI), spheres mark the Cα positions of residues crosslinked to HLA-II. An HLA-II molecule may approach from either side 1 (orange) or side 2 (purple). Occupancy volumes calculated by DisVis are shown in orange and purple. **(C, D)** Highest-scoring docking models for side 1 (C) and side 2 (D) respectively. Red spheres represent Cα of crosslinked positions connected by SASDs (black tube).

of crosslinking restraints summarizing the contact regions between HLA-I and HLA-II. This includes, for instance, equivalent links between position 92 on HLA-A to position 64 on HLA-DRα and to the equivalent position 65 on HLA-DQα (Supplementary Table A.3). In particular, the flexible new N-terminus of HLA-IIβ, after cleavage of the signal peptide, appears to be proximal to HLA-I, as supported by multiple crosslinks (Fig. 3D).

Although it is succinct to visualize these consolidated crosslinks on linear HLA-I and HLA-II protein sequences (Fig. 3D), distant regions in the sequence may still be in close spatial proximity considering the three-dimensional protein structures. As such, summarizing these restraints into possible modes of interaction would be critical for structural

modeling of these complexes. To this end, we next marked the crosslinked residues on a 3D structure of HLA-II, and observed that all the residues crosslinked to HLA-I are located on the same side of HLA-II (Supplementary Fig. A.5). This suggests that HLA-II likely approaches HLA-I through one contact surface on one side of HLA-II (one mode of interaction from HLA-II to HLA-I). On the contrary, crosslinked positions mapped on the structure of HLA-I were not one-directional (Fig. 4B), suggesting that the crosslinking restraints likely cannot be satisfied all at once by one mode of interaction. Indeed, DisVis (van Zundert et al., 2017; van Zundert and Bonvin, 2015) analysis revealed two possible modes of interaction (from HLA-I to HLA-II) that would collectively best satisfy the crosslinking restraints obtained experimentally. In one mode of interaction (side 1), HLA-I residues in orange could be linked to HLA-II, and in the second mode of interaction (side 2), HLA-I residues in purple (Fig. 4B) could be linked to likely another molecule of HLA-II (Supplementary Table A.3). It is key to note that in this model, one molecule of HLA-I need not interact with two molecules of HLA-II simultaneously. Taken together, our crosslinking evidence and modeling suggest that HLA-II has a single interacting interface with HLA-I, whereas HLA-I could interact with HLA-II via either one of the two inferred interacting surfaces (side 1 and side 2, Fig. 4B).

By performing molecular docking with HADDOCK (van Zundert et al., 2016) using these two sets of distance restraints, together with a further restraint for the membrane protein orientation (since HLA peptide loading grooves should always be outward-facing), we retrieved 200 docking models each for side 1 and side 2, which were scored and clustered by HADDOCK. Since HADDOCK uses Euclidean distance as a restraint, the models with the best HADDOCK score will have no overlength Euclidean distances but could still have an overlength SASD. We thus ranked the docking models additionally by means of cMNXL scores, which were calculated based on SASDs with XLM tools (Sinnott et al., 2020) (Supplementary Fig. A.6). The top cMNXL scoring models were also members of the high scoring HADDOCK clusters, suggesting these are indeed the best models based on our data. With these considerations, we arrived at two potential HLA-I to HLA-II docking models (side 1 in Fig. 4C; side 2 in Fig. 4D).

Hence, based on our plasma membrane XL-MS data we can conclude that HLA molecules interact with each other on the plasma membrane of the antigen presenting cell. By using structural docking, we can also better describe the nature of these HLA-I – HLA-II interactions within the plasma membrane environment of whole cells. HLA-II likely has a single interaction interface with HLA-I that consists predominantly of HLA-IIα and the N-terminus of the HLA-IIβ, whereas HLA-I could engage HLA-II via one of two different modes of interactions. The first is from the side of the β2M whereas the second is from the side of the Ig-like domain (Fig. 4C, D). Both modes of interaction involve the rims of the peptide binding domain of HLA-I but since the interaction interfaces are sufficiently far apart, we cannot rule out a scenario where both modes of interaction could occur simultaneously (Supplementary Fig. A.7).

4. Discussion

In mammalian cells, the fine diversity in signaling outcomes far exceeds the number of signaling proteins or pathways we know, and assembly into protein complexes is one of the most important means to expand signaling intricacy (Bludau and Aebersold, 2020). The plasma membrane of each cell is particularly crucial as a signaling interface with other cell types, which is, for instance, also constantly screened by the immune system for signs of infection or poor health. Despite these obvious incentives to better characterize the external cell surface, native protein-protein interactions in the plasma membrane are notoriously difficult to preserve, and could be easily lost during protein solubilization with detergents or become fundamentally changed when isolated from the membrane milieu. As such, the consensus approach to this challenge in the scientific community has been to isolate and purify as little as possible before analysis readout. This is evident from the concerted efforts into perfecting techniques such as FRET (Santos et al., 2015), protein-fragment complementation assays (Fujii et al., 2018), super-resolution light microscopy (Pi et al., 2014), and cryo electron microscopy (Lučić et al., 2013), to investigate plasma membrane protein-protein interactions.

In this work, we performed extracellular plasma membrane crosslinking, starting from intact cells, with the goal of preserving protein-protein interactions in the plasma membrane. The DSSO chemical crosslinking was performed in physiological pH and solvent environment to best preserve extracellular protein-protein interactions, before a double-purification for plasma membranes and crosslinked peptides was performed. With such a strategy any sample preparation steps after crosslinking would not introduce structural artefacts, thereby providing native structural information in a manner similar to cryo-electron microscopy of intact cells (Irobalieva et al., 2016; Schaffer et al., 2017). Using this approach, we could detect a large number of crosslinks that exemplify native protein-protein interactions on the cell exterior, without protein tagging or over-expression. We also verified that many of these crosslinks conformed to the documented crystal structures, and that SASDs of these crosslinks on these structures are within the DSSO length constraints (Fig. 2 and supplementary Fig. A.1).

With a set of distance restraints revealed by DSSO crosslinking of JY cells, we delved deep into the HLA-centric cell-surface interactome. Such an extensive HLA-interactome profiling is one of its kind, and provides exquisite information to delineate the cell surface terrain and architecture surrounding HLA molecules, which are known to be crucial determinants of T-cell recognition and binding (Cole et al., 2017; Gao et al., 1997; Yin et al., 2012). Interestingly, we found HLA proteins to be prominently interacting with other HLA proteins within and between classes I and II. Such interactions have been postulated, sporadically verified, and shown to be frequent and abundant on the cell membrane (Bene et al., 1994; Jenei et al., 1997; Szöllósi et al., 1996; Szöllösi et al., 1989), that might also have functional consequences on T-cell recognition (Anikeeva et al., 2019; Fooksman et al., 2006). However, to our knowledge, these interactions were never investigated systematically with site-specific resolution. More importantly, using a combination of modeling tools, we could summarize the modes of interaction between HLA-I and HLA-II molecules, and determine the interaction interfaces in these complexes, relying only on the endogenous HLA expression and interactions. In addition, with sequence-specific evidence in the form of crosslinked peptide pairs, we could further demonstrate that different HLA-I allotypes engage in the same kind of interactions interchangeably.

A dominant mode of interaction between HLA-I proteins, however, could not be resolved using only crosslinking information acquired herein. This may suggest that more structural variants exist in the HLA-I multimers, such that co-occurring multimers of HLA-I may be too diverse to characterize individually using this methodology. Indeed, heterogenous clusters of HLA-I complexes in the cell membrane have been suggested (Bodnár et al., 2003), where some HLA-I molecules in the cluster are a free heavy chain, lacking the β2M subunit (Dirscherl et al., 2018), thereby introducing additional structural diversity in the interactions between HLA-I molecules. The XL-MS methodology cannot, a priori, distinguish between a free HLA-I heavy chain and a full HLA-I complex since they have exactly the same sequence. Therefore, structural modelling of the HLA-I – HLA-I modes of interaction would still require complementary structural data obtained by other methods. It is also important to note that lack of crosslinks on a certain region or domain does no directly imply lack of interaction, and may also be due to the lack of crosslink-able lysine residues.

Intriguingly, by aligning the docking complexes of HLA-I and HLA-II with the structures of CD8, CD4 and their respective TCRs (Supplementary Figs. A.8, A.9), we noticed that, according to our models, some of these proteins cannot simultaneously engage in interactions with HLA molecules. The binding interfaces of HLA-II (on side 2, but not on side 1) and CD8 on HLA-I overlap, and as a result HLA-II and CD8 cannot bind HLA-I simultaneously. We also noticed that HLA-II (on side 2, but not on

side 1) cannot engage HLA-I and the TCR at the same time. These observations seem to imply that specific interaction configurations between HLA molecules may functionally preclude TCR binding, or vice versa, albeit these hypotheses require more experimental verification. With further improvements in sensitivity, we could envision that in future experiments we might be able to structurally map the immunological synapse between a T-cell and an antigen presenting cell.

In summary, here we present orthogonal structural information to support and reconcile previously reported hints of multimeric HLA assemblies present on the cell surface. Using extracellular chemical crosslinking on whole cells, we show that we could directly retrieve a large set of extracellular crosslinking restraints, to model cell-surface interactions. We envision that using this approach, many more plasma membrane complexes could be studied in a similar manner. Even for membrane proteins with lower endogenous expression levels, the same approach may still be feasible, by replacing the plasma membrane isolation step with immunoaffinity purification, which would improve the crosslinking coverage of the desired complexes. This may also further boost specificity when only a single protein complex is to be studied in greater detail.

Data availability

The mass spectrometry proteomics data, sequence database, and table of CSMs have been deposited to the ProteomeXchange Consortium via the PRIDE (Perez-Riverol et al., 2019) partner repository with the dataset identifier PXD022675. The coordinates of the docking models along with the restraints used to generate these have been deposited to PDB-Dev repository with entry ID PDBDEV_00000066.

Funding

GA was supported by the Human Frontier Science Program (long term fellowship LT000086/2018-L). AJRH acknowledges the Dutch Research Council (NWO) for partly supporting this work through the NWO TA project 741.018.201.

CRediT authorship contribution statement

Gad Armony: Conceptualization, Methodology, Validation, Formal analysis, Investigation, Data curation, Writing - original draft, Visualization, Supervision, Funding acquisition. **Albert J.R. Heck:** Conceptualization, Resources, Writing - review & editing, Supervision, Funding acquisition. **Wei Wu:** Conceptualization, Methodology, Investigation, Writing - original draft, Writing - review & editing, Visualization, Supervision.

Declaration of Competing Interest

The authors declare no conflict of interest.

Acknowledgments

We thank our lab members Dominique Hagemans for support with SCX fractionation, Barbara Steigenberger for synthesizing the DSSO used in this study, and Julia Bauzá-Martinez and Laura C Demmers for providing whole-cell proteome data for JY cells. The W6/32 antibody was a kind gift from Prof. Dr. Stefan Stevanović (Department of Immunology, Tübingen). We also thank Alexandre M.J.J. Bonvin (Utrecht University), the HADDOCK team, and WeNMR Grid for providing HADDOCK and Dis-Vis web services.

Appendix A. Supplementary data

Supplementary material related to this article can be found, in the online version, at doi:https://doi.org/10.1016/j.molimm.2021.05.010.

References

Albanese, P., Tamara, S., Saracco, G., Scheltema, R.A., Pagliano, C., 2020. How paired PSII–LHCII supercomplexes mediate the stacking of plant thylakoid membranes unveiled by structural mass-spectrometry. Nat. Commun. 11, 1361. https://doi.org/10.1038/s41467-020-15184-1.

Alcover, A., Alarcón, B., Di Bartolo, V., 2018. Cell biology of T cell receptor expression and regulation. Annu. Rev. Immunol. 36, 103–125. https://doi.org/10.1146/annurev-immunol-042617-053429.

Anikeeva, N., Fischer, N.O., Blanchette, C.D., Sykulev, Y., 2019. Extent of MHC clustering regulates selectivity and effectiveness of t cell responses. J. Immunol. 202, 591–597. https://doi.org/10.4049/jimmunol.1801196.

Bartolec, T.K., Smith, D.-L., Pang, C.N.I., Xu, Y.D., Hamey, J.J., Wilkins, M.R., 2020. Cross-linking mass spectrometry analysis of the yeast nucleus reveals extensive protein−protein interactions not detected by systematic two-hybrid or affinity purification-mass spectrometry. Anal. Chem. 9 https://doi.org/10.1021/acs.analchem.9b03975.

Bene, L., Balázs, M., Matkó, J., Möst, J., Dierich, M.P., Szöllsi, J., Damjanovich, S., 1994. Lateral organization of the ICAM-1 molecule at the surface of human lymphoblasts: a possible model for its co-distribution with the IL-2 receptor, class I and class II HLA molecules. Eur. J. Immunol. 24, 2115–2123. https://doi.org/10.1002/eji.1830240928.

Bludau, I., Aebersold, R., 2020. Proteomic and interactomic insights into the molecular basis of cell functional diversity. Nat. Rev. Mol. Cell Biol. 21, 327–340. https://doi.org/10.1038/s41580-020-0231-2.

Bodnár, A., Bacsó, Z., Jenei, A., Jovin, T.M., Edidin, M., Damjanovich, S., Matkó, J., 2003. Class I HLA oligomerization at the surface of B cells is controlled by exogenous β2-microglobulin: implications in activation of cytotoxic T lymphocytes. Int. Immunol. 15, 331–339. https://doi.org/10.1093/intimm/dxg042.

Bullock, J.M.A., Schwab, J., Thalassinos, K., Topf, M., 2016. The importance of non-accessible crosslinks and solvent accessible surface distance in modeling proteins with restraints from crosslinking mass spectrometry. Mol. Cell. Proteom. 15, 2491–2500. https://doi.org/10.1074/mcp.M116.058560.

Chavez, J.D., Lee, C.F., Caudal, A., Keller, A., Tian, R., Bruce, J.E., 2018. Chemical crosslinking mass spectrometry analysis of protein conformations and supercomplexes in heart tissue. Cell Syst. 6, 136–141. https://doi.org/10.1016/j.cels.2017.10.017 e5.

Chen, Z.A., Jawhari, A., Fischer, L., Buchen, C., Tahir, S., Kamenski, T., Rasmussen, M., Lariviere, L., Bukowski-Wills, J.C., Nilges, M., Cramer, P., Rappsilber, J., 2010. Architecture of the RNA polymerase II-TFIIF complex revealed by cross-linking and mass spectrometry. EMBO J. 29, 717–726. https://doi.org/10.1038/emboj.2009.401.

Cole, D.K., Fuller, A., Dolton, G., Zervoudi, E., Legut, M., Miles, K., Blanchfield, L., Madura, F., Holland, C.J., Bulek, A.M., Bridgeman, J.S., Miles, J.J., Schauenburg, A. J.A., Beck, K., Evavold, B.D., Rizkallah, P.J., Sewell, A.K., 2017. Dual molecular mechanisms govern escape at immunodominant HLA A2-Restricted HIV epitope. Front. Immunol. 8, 1503. https://doi.org/10.3389/fimmu.2017.01503.

Combe, C.W., Fischer, L., Rappsilber, J., 2015. xiNET: cross-link network maps with residue resolution. Mol. Cell. Proteom. 14, 1137–1147. https://doi.org/10.1074/mcp.O114.042259.

Cui, Y., Zhang, X., Yu, M., Zhu, Y., Xing, J., Lin, J., 2019. Techniques for detecting protein-protein interactions in living cells: principles, limitations, and recent progress. Sci. China Life Sci. 62, 619–632. https://doi.org/10.1007/s11427-018-9500-7.

de Graaf, S.C., Klykov, O., van den Toorn, H., Scheltema, R.A., 2019. Cross-ID: analysis and visualization of complex XL–MS-Driven protein interaction networks. J. Proteome Res. 18, 642–651. https://doi.org/10.1021/acs.jproteome.8b00725.

Dirscherl, C., Hein, Z., Ramnarayan, V.R., Jacob-Dolan, C., Springer, S., 2018. A two-hybrid antibody micropattern assay reveals specific in cis interactions of MHC I heavy chains at the cell surface. eLife 7, e34150. https://doi.org/10.7554/eLife.34150.

Fernandez-Martinez, J., Kim, S.J., Shi, Y., Upla, P., Pellarin, R., Gagnon, M., Chemmama, I.E., Wang, J., Nudelman, I., Zhang, W., Williams, R., Rice, W.J., Stokes, D.L., Zenklusen, D., Chait, B.T., Sali, A., Rout, M.P., 2016. Structure and function of the nuclear pore complex cytoplasmic mRNA export platform. Cell 167, 1215–1228. https://doi.org/10.1016/j.cell.2016.10.028 e25.

Fooksman, D.R., Grönvall, G.K., Tang, Q., Edidin, M., 2006. Clustering class I MHC modulates sensitivity of t cell recognition. J. Immunol. 176, 6673–6680. https://doi.org/10.4049/jimmunol.176.11.6673.

Fritzsche, R., Ihling, C.H., Götze, M., Sinz, A., 2012. Optimizing the enrichment of cross-linked products for mass spectrometric protein analysis. Rapid Commun. Mass Spectrom. 26, 653–658. https://doi.org/10.1002/rcm.6150.

Fujii, Y., Yoshimura, A., Kodama, Y., 2018. A novel orange-colored bimolecular fluorescence complementation (BiFC) assay using monomeric Kusabira-Orange protein. BioTechniques 64, 153–161. https://doi.org/10.2144/btn-2017-0121.

Fürsch, J., Kammer, K.-M., Kreft, S.G., Beck, M., Stengel, F., 2020. Proteome-wide structural probing of low-abundant protein interactions by cross-linking mass spectrometry. Anal. Chem. 92, 4016–4022. https://doi.org/10.1021/acs.analchem.9b05559.

Gao, G.F., Tormo, J., Gerth, U.C., Wyer, J.R., McMichael, A.J., Stuart, D.I., Bell, J.I., Jones, E.Y., Jakobsen, B.K., 1997. Crystal structure of the complex between human CD8αα and HLA-A2. Nature 387, 630–634. https://doi.org/10.1038/42523.

Gurevich, V.V., Gurevich, E.V., 2017. Molecular mechanisms of GPCR signaling: a structural perspective. Int. J. Mol. Sci. 18 https://doi.org/10.3390/ijms18122519.

Huttlin, E.L., Bruckner, R.J., Paulo, J.A., Cannon, J.R., Ting, L., Baltier, K., Colby, G., Gebreab, F., Gygi, M.P., Parzen, H., Szpyt, J., Tam, S., Zarraga, G., Pontano-

Vaites, L., Swarup, S., White, A.E., Schweppe, D.K., Rad, R., Erickson, B.K., Obar, R. A., Guruharsha, K.G., Li, K., Artavanis-Tsakonas, S., Gygi, S.P., Harper, J.W., 2017. Architecture of the human interactome defines protein communities and disease networks. Nature 545, 505–509. https://doi.org/10.1038/nature22366.

Huttlin, E.L., Bruckner, R.J., Navarrete-Perea, J., Cannon, J.R., Baltier, K., Gebreab, F., Gygi, M.P., Thornock, A., Zarraga, G., Tam, S., Szpyt, J., Panov, A., Parzen, H., Fu, S., Golbazi, A., Maenpaa, E., Stricker, K., Thakurta, S.G., Rad, R., Pan, J., Nusinow, D.P., Paulo, J.A., Schweppe, D.K., Vaites, L.P., Harper, J.W., Gygi, S.P., 2020. Dual proteome-scale networks reveal cell-specific remodeling of the human interactome. bioRxiv. https://doi.org/10.1101/2020.01.19.905109, 2020.01.19.905109.

Irobalieva, R.N., Martins, B., Medalia, O., 2016. Cellular structural biology as revealed by cryo-electron tomography. J. Cell. Sci. 129, 469–476. https://doi.org/10.1242/jcs.171967.

Jenei, A., Varga, S., Bene, L., Mátyus, L., Bodnár, A., Bacsó, Z., Pieri, C., Gáspár, R., Farkas, T., Damjanovich, S., 1997. HLA class I and II antigens are partially co-clustered in the plasma membrane of human lymphoblastoid cells. PNAS 94, 7269–7274. https://doi.org/10.1073/pnas.94.14.7269.

Klykov, O., van der Zwaan, C., Heck, A.J.R., Meijer, A.B., Scheltema, R.A., 2020. Missing regions within the molecular architecture of human fibrin clots structurally resolved by XL-MS and integrative structural modeling. PNAS 117, 1976–1987. https://doi.org/10.1073/pnas.1911785117.

Lavi, Y., Gov, N., Edidin, M., Gheber, L.A., 2012. Lifetime of major histocompatibility complex Class-I membrane clusters is controlled by the actin cytoskeleton. Biophys. J. 102, 1543–1550. https://doi.org/10.1016/j.bpj.2012.01.042.

Lebedeva, T., Anikeeva, N., Kalams, S.A., Walker, B.D., Gaidarov, I., Keen, J.H., Sykulev, Y., 2004. Major histocompatibility complex class I–intercellular adhesion molecule-1 association on the surface of target cells: implications for antigen presentation to cytotoxic T lymphocytes. Immunology 113, 460–471. https://doi.org/10.1111/j.1365-2567.2004.01985.x.

Leitner, A., Joachimiak, L.A., Bracher, A., Mönkemeyer, L., Walzthoeni, T., Chen, B., Pechmann, S., Holmes, S., Cong, Y., Ma, B., Ludtke, S., Chiu, W., Hartl, F.U., Aebersold, R., Frydman, J., 2012. The molecular architecture of the eukaryotic chaperonin TRiC/CCT. Structure 20, 814–825. https://doi.org/10.1016/j.str.2012.03.007.

Liu, F., Lössl, P., Scheltema, R., Viner, R., Heck, A.J.R., 2017. Optimized fragmentation schemes and data analysis strategies for proteome-wide cross-link identification. Nat. Commun. 8, 15473. https://doi.org/10.1038/ncomms15473.

Liu, F., Lössl, P., Rabbitts, B.M., Balaban, R.S., Heck, A.J.R., 2018a. The interactome of intact mitochondria by cross-linking mass spectrometry provides evidence for coexisting respiratory supercomplexes. Mol. Cell. Proteom. 17, 216–232. https://doi.org/10.1074/mcp.RA117.000470.

Liu, S., Yu, F., Hu, Q., Wang, T., Yu, L., Du, S., Yu, W., Li, N., 2018b. Development of in planta chemical cross-linking-Based quantitative interactomics in Arabidopsis. J. Proteome Res. 17, 3195–3213. https://doi.org/10.1021/acs.jproteome.8b00320.

Lučić, V., Rigort, A., Baumeister, W., 2013. Cryo-electron tomography: the challenge of doing structural biology in situ. J. Cell Biol. 202, 407–419. https://doi.org/10.1083/jcb.201304193.

Madeira, F., Park, Y. mi, Lee, J., Buso, N., Gur, T., Madhusoodanan, N., Basutkar, P., Tivey, A.R.N., Potter, S.C., Finn, R.D., Lopez, R., 2019. The EMBL-EBI search and sequence analysis tools APIs in 2019. Nucleic Acids Res. 47, W636–W641. https://doi.org/10.1093/nar/gkz268.

Matko, J., Bushkin, Y., Wei, T., Edidin, M., 1994. Clustering of class I HLA molecules on the surfaces of activated and transformed human cells. J. Immunol. 152, 3353–3360.

Mezzadra, R., Sun, C., Jae, L.T., Gomez-Eerland, R., de Vries, E., Wu, W., Logtenberg, M. E.W., Slagter, M., Rozeman, E.A., Hofland, I., Broeks, A., Horlings, H.M., Wessels, L. F.A., Blank, C.U., Xiao, Y., Heck, A.J.R., Borst, J., Brummelkamp, T.R., Schumacher, T.N.M., 2017. Identification of CMTM6 and CMTM4 as PD-L1 protein regulators. Nature 549, 106–110. https://doi.org/10.1038/nature23669.

Neumann, F., Kaddu-Mulindwa, D., Widmann, T., Preuss, K.-D., Held, G., Zwick, C., Roemer, K., Pfreundschuh, M., Kubuschok, B., 2013. EBV-transformed lymphoblastoid cell lines as vaccines against cancer testis antigen-positive tumors. Cancer Immunol. Immunother. 62, 1211–1222. https://doi.org/10.1007/s00262-013-1412-z.

Perez-Riverol, Y., Csordas, A., Bai, J., Bernal-Llinares, M., Hewapathirana, S., Kundu, D. J., Inuganti, A., Griss, J., Mayer, G., Eisenacher, M., Pérez, E., Uszkoreit, J., Pfeuffer, J., Sachsenberg, T., Yılmaz, Ş., Tiwary, S., Cox, J., Audain, E., Walzer, M., Jarnuczak, A.F., Ternent, T., Brazma, A., Vizcaíno, J.A., 2019. The PRIDE database and related tools and resources in 2019: improving support for quantification data. Nucleic Acids Res. 47, D442–D450. https://doi.org/10.1093/nar/gky1106.

Pi, J., Jin, H., Yang, F., Chen, Z.W., Cai, J., 2014. In situ single molecule imaging of cell membranes: linking basic nanotechniques to cell biology, immunology and medicine. Nanoscale 6, 12229–12249. https://doi.org/10.1039/C4NR04195J.

Rinner, O., Seebacher, J., Walzthoeni, T., Mueller, L., Beck, M., Schmidt, A., Mueller, M., Aebersold, R., 2008. Identification of cross-linked peptides from large sequence databases. Nat. Methods 5, 315–318. https://doi.org/10.1038/nmeth.1192.

Santos, C.D.L., Chang, C.-W., Mycek, M.-A., Cardullo, R.A., 2015. FRAP, FLIM, and FRET: detection and analysis of cellular dynamics on a molecular scale using fluorescence microscopy. Mol. Reprod. Dev. 82, 587–604. https://doi.org/10.1002/mrd.22501.

Schaffer, M., Mahamid, J., Engel, B.D., Laugks, T., Baumeister, W., Plitzko, J.M., 2017. Optimized cryo-focused ion beam sample preparation aimed at in situ structural studies of membrane proteins. Journal of Structural Biology, Electron Tomography 197, 73–82. https://doi.org/10.1016/j.jsb.2016.07.010.

Sinnott, M., Malhotra, S., Madhusudhan, M.S., Thalassinos, K., Topf, M., 2020. Combining information from crosslinks and monolinks in the modeling of protein structures. Structure 28, 1061–1070. https://doi.org/10.1016/j.str.2020.05.012 e3.

Staros, J.V., 1982. N-hydroxysulfosuccinimide active esters: bis(N-hydroxysulfosuccinimide) esters of two dicarboxylic acids are hydrophilic, membrane-impermeant, protein cross-linkers. Biochemistry 21, 3950–3955. https://doi.org/10.1021/bi00260a008.

Sun, Z., Guo, S.S., Fässler, R., 2016. Integrin-mediated mechanotransduction. J. Cell Biol. 215, 445–456. https://doi.org/10.1083/jcb.201609037.

Szöllösi, J., Damjanovich, S., Balàzs, M., Nagy, P., Trón, L., Fulwyler, M.J., Brodsky, F. M., 1989. Physical association between MHC class I and class II molecules detected on the cell surface by flow cytometric energy transfer. J. Immunol. 143, 208–213.

Szöllósi, J., Horejsí, V., Bene, L., Angelisová, P., Damjanovich, S., 1996. Supramolecular complexes of MHC class I, MHC class II, CD20, and tetraspan molecules (CD53, CD81, and CD82) at the surface of a B cell line JY. J. Immunol. 157, 2939–2946.

Tüting, C., Iacobucci, C., Ihling, C.H., Kastritis, P.L., Sinz, A., 2020. Structural analysis of 70S ribosomes by cross-linking/mass spectrometry reveals conformational plasticity. Sci. Rep. 10, 12618. https://doi.org/10.1038/s41598-020-69313-3.

van Zundert, G.C.P., Bonvin, A.M.J.J., 2015. DisVis: quantifying and visualizing accessible interaction space of distance-restrained biomolecular complexes. Bioinformatics 31, 3222–3224. https://doi.org/10.1093/bioinformatics/btv333.

van Zundert, G.C.P., Rodrigues, J.P.G.L.M., Trellet, M., Schmitz, C., Kastritis, P.L., Karaca, E., Melquiond, A.S.J., van Dijk, M., de Vries, S.J., Bonvin, A.M.J.J., 2016. The HADDOCK2.2 web server: user-friendly integrative modeling of biomolecular complexes. J. Mol. Biol., Comput. Res. Mol. Biol. 428, 720–725. https://doi.org/10.1016/j.jmb.2015.09.014.

van Zundert, G.C.P., Trellet, M., Schaarschmidt, J., Kurkcuoglu, Z., David, M., Verlato, M., Rosato, A., Bonvin, A.M.J.J., 2017. The DisVis and PowerFit web servers: explorative and integrative modeling of biomolecular complexes. J. Mol. Biol., Comput. Res. Mol. Biol. 429, 399–407. https://doi.org/10.1016/j.jmb.2016.11.032.

Vreven, T., Schweppe, D.K., Chavez, J.D., Weisbrod, C.R., Shibata, S., Zheng, C., Bruce, J. E., Weng, Z., 2018. Integrating cross-linking experiments with ab initio protein–Protein docking. J. Mol. Biol. 430, 1814–1828. https://doi.org/10.1016/j.jmb.2018.04.010.

Webb, B., Sali, A., 2016. Comparative protein structure modeling using MODELLER. Curr. Protoc. Bioinformatics 54, 5.6.1–5.6.37. https://doi.org/10.1002/cpbi.3.

Yang, J., Yan, R., Roy, A., Xu, D., Poisson, J., Zhang, Y., 2015. The I-TASSER Suite: protein structure and function prediction. Nat. Methods 12, 7–8. https://doi.org/10.1038/nmeth.3213.

Yin, Y., Wang, X.X., Mariuzza, R.A., 2012. Crystal structure of a complete ternary complex of T-cell receptor, peptide-MHC, and CD4. Proc. Natl. Acad. Sci. U. S. A. 109, 5405–5410. https://doi.org/10.1073/pnas.1118801109.

Zhang, Q., Cherezov, V., 2019. Chemical tools for membrane protein structural biology. Curr Opin Struct Biol. 58, 278–285. https://doi.org/10.1016/j.sbi.2019.06.002.